Journal of ELECTRONIC MATERIALS, Vol. 47, No. 4, 2018
https://doi.org/10.1007/s11664-017-6038-z

Intermetallic Growth Induced Large-Scale Void Growth and Cracking Failure in Line-Type Cu/Solder/Cu Joints Under Current Stressing

ZHUO CHEN,[1] WENYA TIAN,[1] JUNHUI LI ,[1,2] and WENHUI ZHU[1]

1.—State Key Laboratory of High Performance Complex Manufacturing, School of Mechanical and Electronical Engineering, Central South University, Changsha 410083, Hunan, China. 2.—e-mail: lijunhui@csu.edu.cn

In order to study the electromigration (EM) behavior of solder joints in electronics packaging, especially under high-current and high-temperature working conditions, line-type Cu/solder/Cu butting samples were prepared to observe the microstructural evolution under 1.0×10^4 A/cm^2 current stressing. A prominent polarity effect was found such that the Cu_6Sn_5 intermetallic compound (IMC) layer at the anode side, which thickened linearly with time, was much thicker than that at the cathode side. Compared to the samples subjected to thermal aging at the same temperature of 180°C, EM enhanced the Cu_3Sn growth at both the anode and the cathode. Two distinct types of damage were observed after extended duration of current stressing. Back-flow of Cu into Cu_3Sn was found at the Cu_3Sn/Cu_6Sn_5 interface of the anode side, causing large voids, while strip cracks developed at the cathode solder/Cu_6Sn_5 interface, causing a significant increase of joint electrical resistance. With the mass transport characteristics that determine the IMC growth and vacancy accumulation analyzed in detail at each interface, formation mechanisms of the two types of damages are discussed.

Key words: Electromigration, intermetallic compounds, solder joint, interfacial mass transport

INTRODUCTION

With the trends for miniaturization and multifunctionalization in electronic products, characteristic sizes of solder joints are decreasing and current density crossing the interconnects of electronic packaging are increasing accordingly. When the downscaling trend pushes the joint size to below 100 μm, especially in three-dimensional integration where the inter-layer connections often consist of microbumps smaller than 50 μm,[1,2] reliability of the solder joints is greatly risked by the unprecedented current density of 1×10^4 A/cm^2 or even higher when in service.[3,4] Under such extreme conditions, atoms in solder joints will have a high mobility to migrate, resulting in void formation and propagation or acceleration of intermetallic compound (IMC) growth, which is commonly known as the electromigration effect.[5–8] As voids and brittle IMCs are most susceptible to structural degradation under multiple external loads, like stress, joule heating or the electric current itself, integrity of the joints ought to be re-examined to incorporate electromigration, particularly in advanced fine-pitch solder interconnections and power electronics, which often face extreme working conditions.

Research on electromigration-induced reliability issues of solder joints is being widely reported, among which a large number of studies have been carried out in flip-chip joints with thin films under bump metal (UBM) stacks, in which the failure mechanism can be either pancake-type voiding or excessive consumption of UBM stacks, depending on the temperature conditions.[9–12] To alleviate the

(Received August 10, 2017; accepted December 21, 2017; published online January 8, 2018)

geometric confinement and microscopic non-uniformity of flip-chip joints, many of the reported studies on fundamental electromigration (EM) characteristics and kinetic features have also been carried out in line-type Cu/solder/Cu joints or Cu-pillar-based microbumps to minimize the effect of current crowding.[13–16] The growth kinetics of IMCs were found to vary significantly from study to study, being heavily influenced by the test structure. This includes the controversy over the growth of Cu_6Sn_5 and Cu_3Sn to be linear or parabolic with time, as well as the exact locations of voids and cracks.[5,13,17–19] On the other hand, experimental studies of solder joint EM have been relatively less reported at temperatures higher than 180°C, while in power electronics packaging, high-temperature working conditions are common.[20,21] Detrimental effects of EM such as large-scale voiding and cracking under such conditions may not be fully exposed by the current research.

In this paper, line-type Cu/Solder/Cu samples were used to investigate the effects of EM on the microstructure evolution. The effect of both current crowding and mechanical stress will be avoided in this line-type structure, allowing the evolution of intermetallics, with the influence of voids and cracks. The samples were stressed with a current density of 1.0×10^4 A/cm^2 for different durations. The growth of the IMCs and the evolutionary process of the damage under such intensified current stressing conditions are discussed and compared with thermal aging at 180°C. The analyses on the basic material behavior and microscopic mechanism on two distinct types of damagesin this study were expected to clarify the kinetic features of IMC growth, as well as to help build a link between the microstructural evolution and failure mechanism inside the solder joint, excluding the influences of joint size and geometry.

EXPERIMENTAL

Line-type Cu/solder/Cu interconnects were prepared with 0.3-mm-diameter straight copper wire (purity: 99.95%) and 0.3-mm-diameter Sn-3.0Ag-0.5Cu solder balls as base materials. The ends of the copper wires were polished flat, perpendicular to the axis. Before soldering, the flat copper wire ends were cleaned by ultrasonic vibration in acetone for 10 s, then dipped into flux to improve solderability. Four solder balls were placed in the middle of a glass capillary, and two Cu wires were inserted from both ends of the capillary. The whole assembly process was carried out in a V-shaped steel groove, as shown in Fig. 1. Afterward, the assembly was heated to 265°C for 10 s using a hot air gun. A force of 1 N was applied from both ends during the soldering. Afterward, the joint was cooled in air to room temperature.

The EM experiments were conducted with a direct current applied to the line-type interconnects

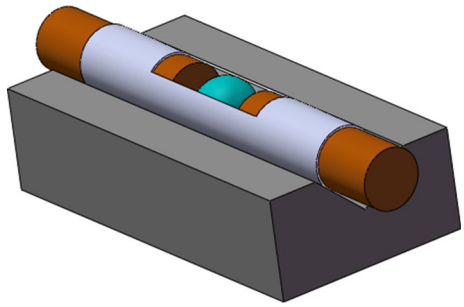

Fig. 1. Schematic of joint preparation.

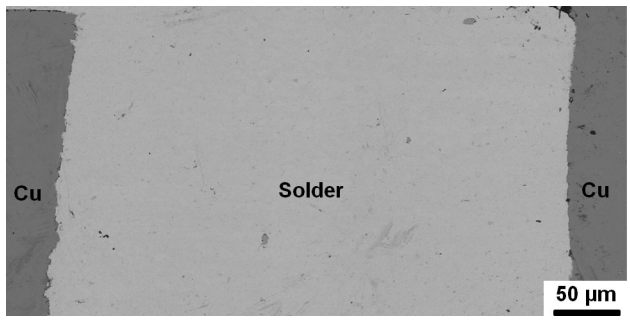

Fig. 2. Cross-sectional SEM image of a butting solder joint before current stessing.

with an applied current density of 1.0×10^4 A/cm^2. Actual temperatures of the joints during current stressing were measured at 180 ± 5°C throughout current applying durations ranging from 0 h to 150 h. In order to compare the effect of current and mere thermal load in the butting solder joint, reference Cu/Solder/Cu specimens were placed in a thermostatic chamber and the temperature was kept at 180°C from 0 h to 150 h. After the EM and thermal aging, the specimens were taken out and cooled in air to room temperature, then sealed within epoxy resin. Finally, the sealed samples were ground and polished along the cross-section perpendicular to the solder joint interface. The microstructural evolution of the line-type interconnects during EM and aging was examined using scanning electron microscopy (SEM); see Fig. 2 for the cross-sectional image of an as-soldered sample using SEM. The width of the solder joints in all the samples was controlled around 450 μm. Energy dispersive x-ray (EDX) spectrometry was used for the identification of the chemical compositions. The areas of the IMC layers were measured with image processing software, and the average thickness of the IMC layers was calculated by dividing the area of IMC with the linear length of the interface.

RESULTS AND DISCUSSION

IMC Morphology and Growth Behavior

Figure 3 shows the joint microstructure throughout the butting joint; two types of Cu-Sn compound

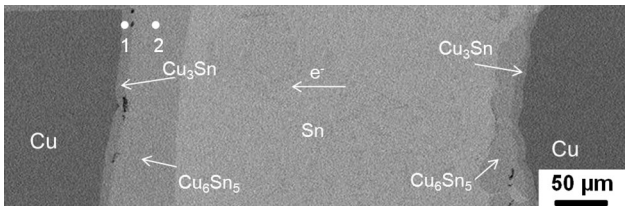

Fig. 3. SEM image of a whole joint showing IMC layers after initial 20 h current stessing.

were observed between the Cu and the solder. Examined by EDX, with atomic percentages of 72.69 Cu and 27.31 Sn at layer 1, and 53.05 Cu and 46.95 Sn at layer 2, the two layers were identified as Cu_3Sn and Cu_6Sn_5, respectively. A prominent polarity effect of IMC growth can be observed with the total IMC thickness being much higher at the anode than that at the cathode after current stressing. Also, the boundaries between the solder/Cu_6Sn_5/Cu_3Sn/Cu phases are wavy at the cathode side, which is in strong contrast with the anode side where the boundaries are much straighter. The wavy profile of the cathode region suggests strong Cu dissolution. Figure 4 shows close-up observations of the interfaces at the anodes and cathodes after the application of 1.0×10^4 A/cm^2 current for various times. Both types of IMCs thickened gradually with increasing EM time at the anode side, as shown in Fig. 5. Cu_3Sn layer thicknesses were found to be similar on both sides after a duration of stressing, and both had slower, linear growth rates at the later stage compared to the initial stage, which will be discussed later. The Cu_6Sn_5 layer at the anode grew following a linear relationship with time.

Unlike the reported research that found that the electric current had a negative effect on the total thickness of the cathode IMCs,[17] here, the current-functioned cathode still has thicker IMCs compared with the thermally aged joints, as seen from the comparison of Fig. 4 with Fig. 6. The solder itself, whether or not containing Cu, could be the cause of this discrepancy. In the thermal aging samples, the growth of the IMCs were far less severe and the change of total thickness of the two IMCs can be expressed by a classical power-law relationship:

$$h_t - h_0 = Kt^n \quad (1)$$

where h_t is the average thickness of the IMC layers at time t, h_0 is the initial thickness ($t = 0$), K is the growth rate constant, and n is the time exponent. In Fig. 7, the linearity of the square of total IMC thickness with aging time suggests the value of n to be around 0.5, consistent with the parabolic growth model in the literature.[22]

Microstructure Deterioration of Joints

As can be seen in Fig. 3 and more specifically clarified in Fig. 8, voids and cracks developed inside

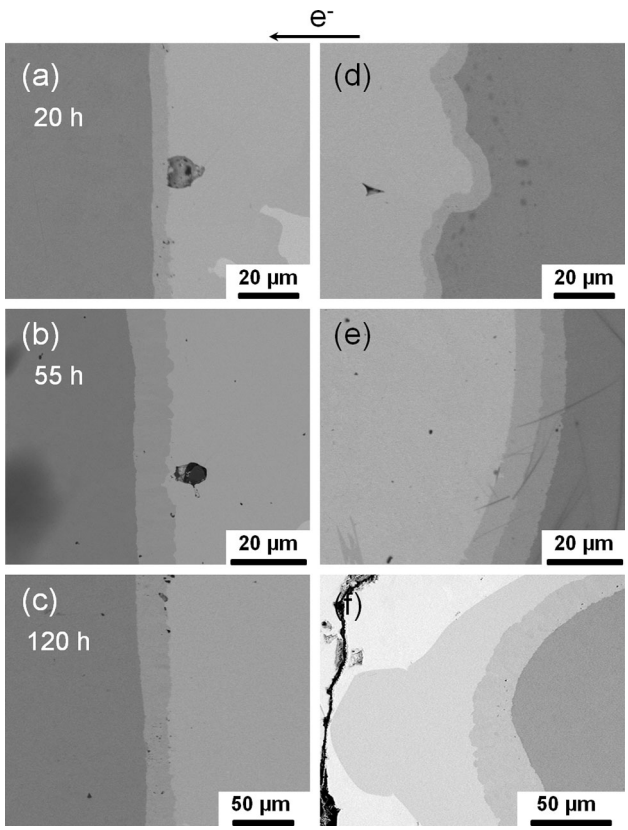

Fig. 4. Close-up SEM micrographs of the solder/Cu interfaces after the application of 1.0×10^4 A/cm^2 current for various times: (a–c) at the anode side, (d–f) at the cathode side.

the joint at certain locations. Circular voids were found to gather at two interfaces: the Cu_3Sn/Cu_6Sn_5 interface at the anode side, and the Cu_6Sn_5/Sn interface at the cathode side. Increased current stressing time led to significantly larger circular voids at the anode side, while at the cathode side, voids were no longer observed in 80-h, and 120-h stressed joints; instead, long strip-like cracks appeared. The development of cracks at the cathode side was presumably following the mechanism described below: after the formation of the initial crack, the current density distribution is altered and local current crowding took place at the tip of the crack due to a geometric singularity. Higher current density then led to accelerated void formation, which encouraged the crack to propagate. Also, the reaction of forming IMCs is a process of total volume shrinkage if we take the joint as a whole,[23] with the tensile stress providing an additional driving force for further cracking. Furthermore, the appearance of cracks would block the electron flow from the cathode to the anode locally, and, as a result, only the region above the crack tip would continue to be subjected to current stressing, at a current density higher than before. Therefore, the profile of solder/IMCs/Cu interfaces were curved (upper right in Fig. 8), due to uneven Cu dissolution along the original interface. The initiation

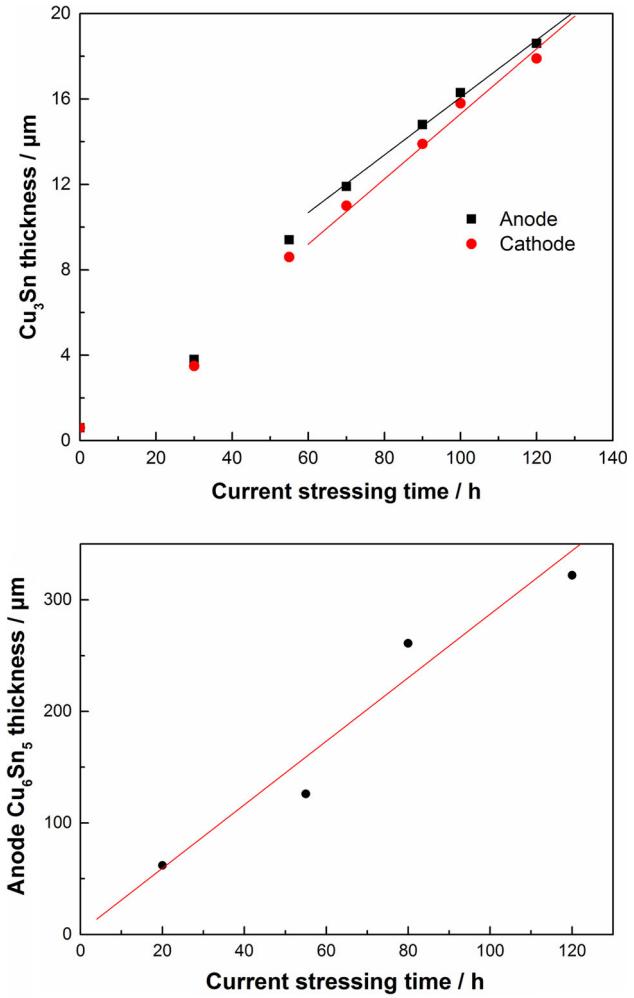

Fig. 5. (a) Thickness of Cu_3Sn at the anode and cathode, and (b) thickness of Cu_6Sn_5 at the anode, after various times of current stressing.

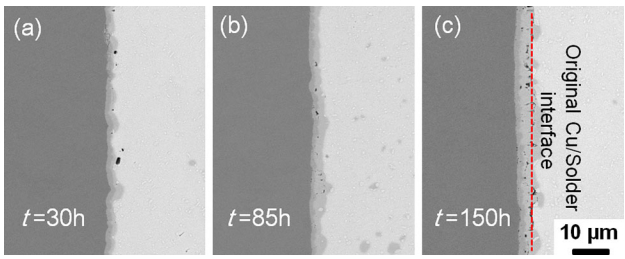

Fig. 6. SEM micrographs of the Cu/solder interfacial IMCs after aging at 180°C for various times.

mechanisms of voids and cracks at each side are detailed in the next section.

Interpretation on the Interfacial Mass Transport During Current Stressing

As is shown in Fig. 9, in the case of Cu_6Sn_5 growth, it should be noted first that the cathode was in a quite dynamic evolution due to Cu dissolution.

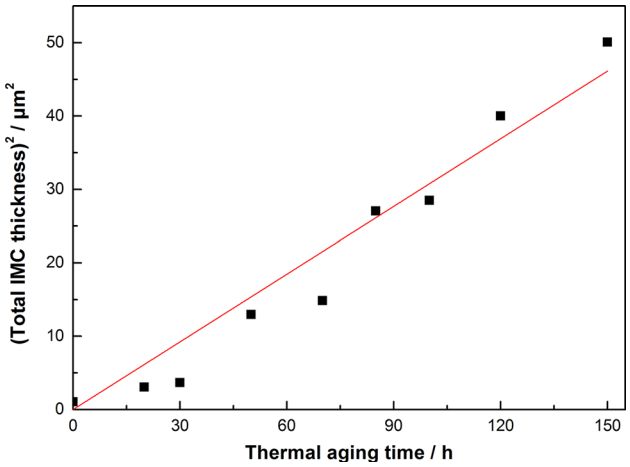

Fig. 7. Variation of interfacial IMC thickness with thermal aging time.

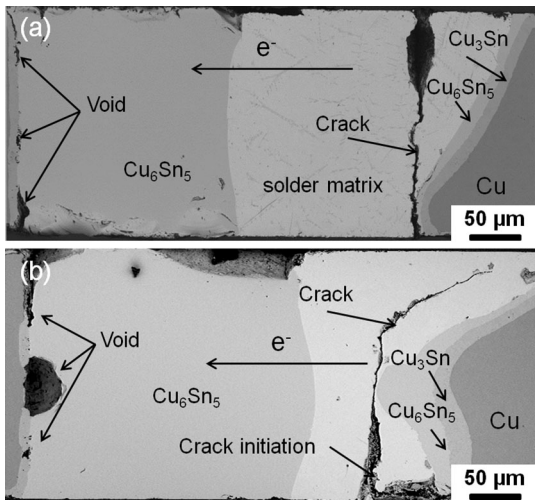

Fig. 8. SEM images of the joints after current stressing for (a) 80 h, and (b) 120 h.

As a result, after current stressing, the Cu_6Sn_5/Cu_3Sn interface and even the Cu_3Sn/Cu interface had moved to the right beyond the original Cu/Sn interface at the cathode side, and sometimes the newly formed interfaces were curved, as discussed earlier. The dissolution of Cu is a reaction-controlled process which means that the dissolution rate is constant. The dissolved Cu atoms, driven by both chemical potential and EM effect, migrated from the cathode to the anode. At the interface between Cu_6Sn_5 and the Sn solder, decomposition of Cu_6Sn_5 took place to release Cu atoms, which transited to the anode side and then precipitated in the form of Cu_6Sn_5. The thickness of the cathode Cu_6Sn_5 phase depended on the interfaces that were moving toward the same direction, making its thickness fluctuate much more with time and difficult to describe compared to the anode case. Throughout the period of current supply, the great majority of the dissolved Cu atoms from the cathode

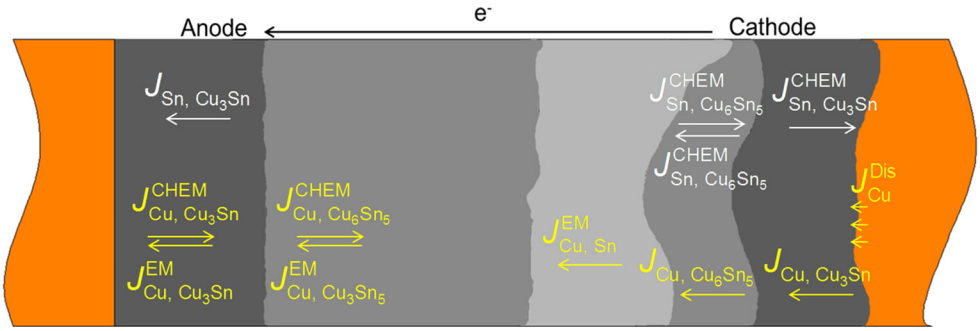

Fig. 9. Schematic of mass transport in a whole joint undergoing EM.

Cu substrate were finally transported across the remaining solder, and thus the growth of Cu_6Sn_5 at the anode is almost linear with time, as shown in Fig. 5b.

The evolution of Cu_3Sn thickness at the anode side is controlled by two interfaces, the first is the Cu/Cu_3Sn interface, which under thermal aging condition has a displacement fitting parabolic rule, controlled by $J^{CHEM}_{Sn,Cu_3Sn} = D_{Sn,Cu_3Sn}\frac{\partial C_{Sn,Cu_3Sn}}{\partial x}$, where D_{Sn,Cu_3Sn} and $\frac{\partial C_{Sn,Cu_3Sn}}{\partial x}$ are the diffusion coefficient and the concentration gradient of Sn in Cu_3Sn, respectively. The other interface is Cu_3Sn/Cu_6Sn_5, which under thermal aging will allow Cu_3Sn to decompose, releasing Cu atoms to Cu_6Sn_5; the exact reason why this interface drifted to the left in Fig. 6c is in accordance with the report by Yang et al.[24] Controlled by $J^{CHEM}_{Cu,Cu_6Sn_5} = D_{Cu,Cu_6Sn_5}\frac{\partial C_{Cu,Cu_6Sn}}{\partial x}$, the rate of this process is also time-dependent. When the Cu/Cu_3Sn interface is superimposed by the effect of constant electrical current, expressed as $J^{EM}_{Sn,Cu_3Sn} = C_{Sn,Cu_3Sn}\frac{D_{Sn,Cu_3Sn}}{kT}Z^*_{Sn,Cu_3Sn}e\rho_{Cu_3Sn}j$, where Z^*_{Sn,Cu_3Sn} is the effective charge number of Sn in Cu_3Sn, e is the electron charge, ρ_{Cu_3Sn} is the density of Cu_3Sn, and j is the current density, the rate of the first process gradually converges to a constant value. At the Cu_3Sn/Cu_6Sn_5 interface, the leftward Cu flux driven by EM, J^{EM}_{Cu,Cu_6Sn_5} reverses the net rightward Cu flux under thermal aging, causing the Cu_3Sn phase to grow even beyond the original soldering interface, at a slight yet stable rate. Thus, linear growth of Cu_3Sn phase after a certain period was observed naturally, as in Fig. 5a. A similar mechanism is expected at the cathode, where the two controlling interfaces of Cu_3Sn move linearly after the concentration gradients around these two interfaces become stable.

It is well known that the formation of both Cu_6Sn_5 and Cu_3Sn IMCs can cause volume shrinkage. Calculated by data from the literature,[25] the reaction of $6Cu + 5Sn \rightarrow Cu_6Sn_5$ causes a 5% shrinkage, and the reaction of $Cu_6Sn_5 + 9Cu \rightarrow 5Cu_3Sn$ causes an additional 4.5% shrinkage. Although the effect of volume change on the void formation and crack propagation in solder joints can be easily seen,

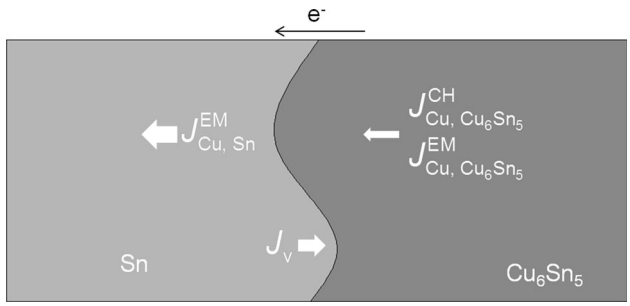

Fig. 10. Schematic of mass transport at the solder/Cu_6Sn_5 interface of the cathode side.

the exact locations of voiding cannot be directly determined. Generally, vacancies are formed where the mass transport rate across a certain interface is discontinuous, and the accumulation of vacancies when not supplied in time results in voids.

In most reported research on thermally aged solder/Cu joints, voids were usually found at two interfaces: the Cu_3Sn/Cu interface, where voids were typically formed by the Kirkendall effect,[26] and the solder/Cu_6Sn_5 interface, where voids were usually exhibited in the form of cracks.[27] However, with the one-directional current applied, an additional driving force was superimposed, causing completely different scenarios compared with thermal aging. In this study, no Kirkendall voids were found near the cathode Cu_3Sn/Cu interface, which is easily understood since the dissolution of the Cu substrate continuously consumed the Kirkendall voiding region. For the solder/Cu_6Sn_5 interface, a tiny region across the interface was considered, as shown in Fig. 10. Due to a certain solubility of Cu in solid Sn, the Cu atoms can diffuse very rapidly in Sn; in fact, the diffusion coefficient $D_{Cu,Sn}$ is four-magnitudes higher than $D_{Cu,\ Cu6Sn5}$.[28] Since the divergence of Cu flux across the interface, $J^{EM}_{Cu,Sn} - (J^{CHEM}_{Cu,Cu_6Sn_5} + J^{EM}_{Cu,Cu_6Sn_5})$, was substantial, local depletion of Cu occurred and vacancies proliferated, which in turn facilitated the dissolution of Cu_6Sn_5, causing this interface to drift rightward. Vacancy accumulation at this region thus initiated the crack.

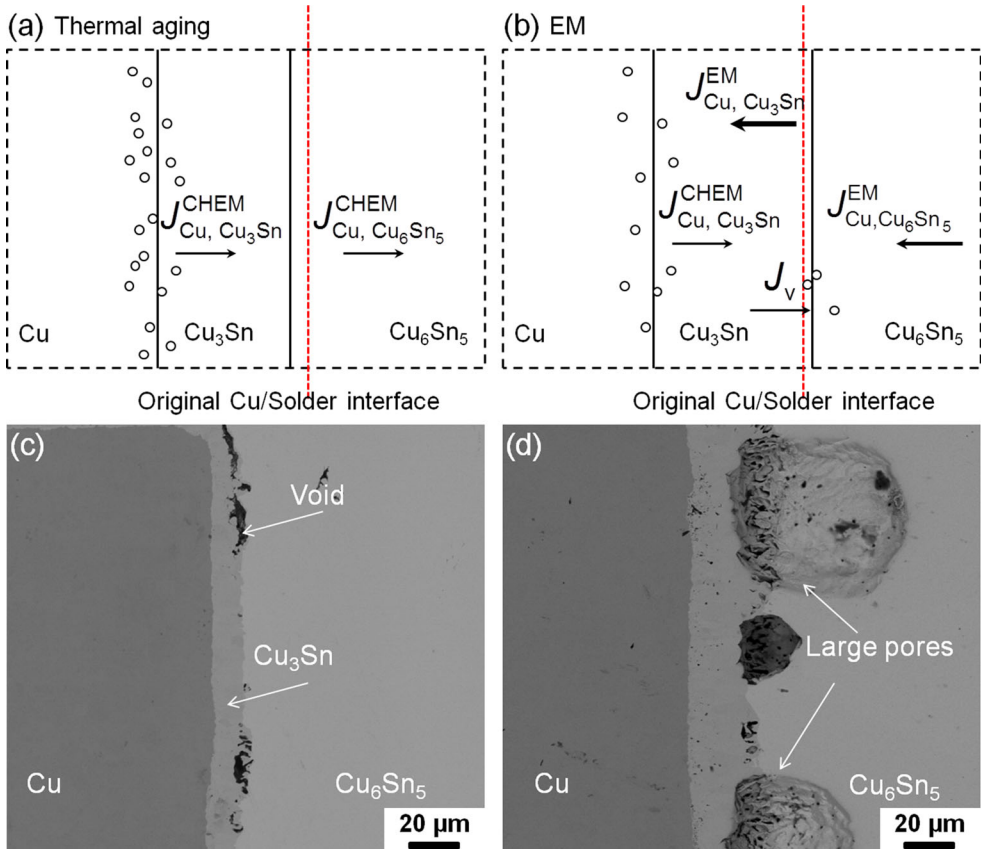

Fig. 11. Schematic of anode-side void formation in (a) thermally aged joints and (b) current-stressed joints; SEM images of the anode region in joints subjected to (c) 1.0×10^4 A/cm^2 and (d) 1.2×10^4 A/cm^2 current.

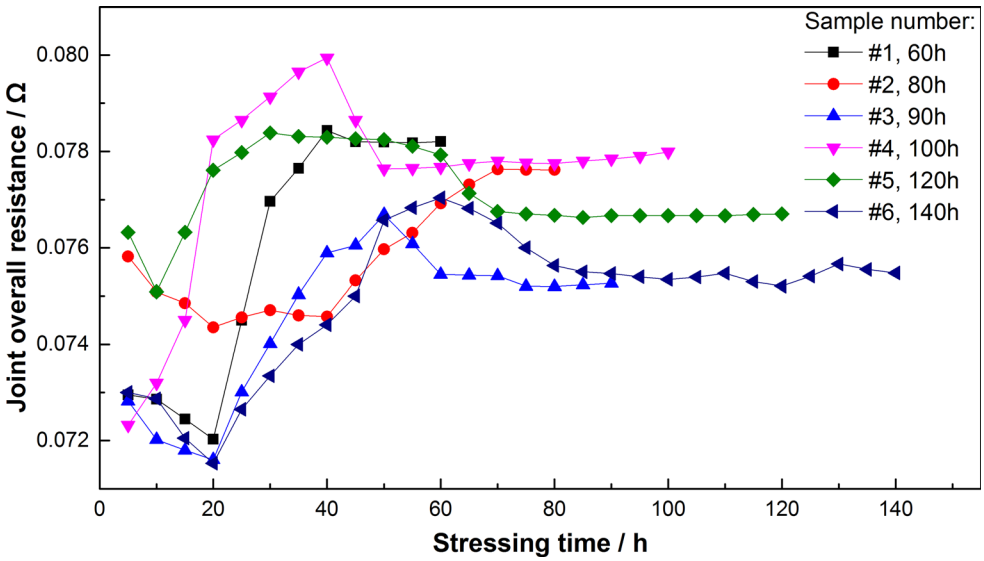

Fig. 12. Electrical resistance curves of each joint stressed at 1.0×10^4 A/cm^2.

At the Cu_3Sn/Cu_6Sn_5 interface of the anode, however, the mechanism of void formation is different. Under the thermal aging condition, Kirkendall voids make the Cu_3Sn/Cu interface porous,[26] as illustrated in Fig. 11a. However, when the interface is subjected to leftward electron flow, Cu flux caused by electromigration is in the opposite direction, which causes net Cu flux leftward, at the expense of Cu in Cu_6Sn_5, as related above. As a result, vacancies flowed rightward to the Cu_3Sn/Cu_6Sn_5

interface, as illustrated in Fig. 11b, and alleviated the Kirkendall voids. The original voids at the Cu/solder interface introduced by incomplete wetting during joint preparation might also have contributed to the observed voids, since the locations of the voids almost stayed the same as before after stressing, seen in Fig. 11c. When the thickness of Cu_3Sn was much thicker under higher stressing temperature, i.e., when the current was 1.2×10^4 A/cm^2 and the remaining solder melted, Cu consumption and volume shrinkage brought about by Cu_3Sn growth became more prominent and could not be timely substituted by sufficient Cu flux at the right end of Fig. 10b. It can be observed in Fig. 11d that large pores of 30–50 μm were found inside the Cu_6Sn_5 phase near this interface. This process took place in a relatively smooth manner, due to the much lower diffusivity of Cu in IMCs than in Sn compared with the cathode case of void formation, producing pores with much lower surface energy and spherical in shape.

Joint Resistance Change Over Current Stressing Time

Figure 12 shows the variation of electrical resistance of a number of samples with time. It can be seen that the value of the resistance from the start, 0.072–0.077 Ω, indistinctly went up in the first 50–70 h, with an average increase of 0.002 Ω. This increase is readily related to the large-scale cracking at the cathode side, and joints would be considered to have failed after such severe damage. Another possible factor that could have caused the resistance change is the evolution of the joint constitution, which can be regarded as a process of IMCs, mainly Cu_6Sn_5, gradually replacing the Cu and the solder. However, based on the resistivity data collected from Refs. 29 and 30, the resistance change caused by IMC formation in a simplified $6Cu + 5\ Sn = Cu_6Sn_5$ reaction should not exceed 0.0004 Ω in all samples at 180°C. After the period of increase, the resistance of all joints gradually stabilized, implying that the cracks no longer propagated with further current stressing, since the evolution of joint microstructure gradually caused the crack tip to be buried inside the solder, instead of being at the solder/Cu_6Sn_5 interface, as shown in Fig. 8.

CONCLUSIONS

In this research, line-type butting solder joints of Cu/solder/Cu were used to investigate the growth of IMCs during EM, as well as the resulting void formation and cracking behavior. The interfacial IMCs at the anode side were thicker than those at the cathode side, and the difference mainly originated from polarized Cu_6Sn_5 growth at the two sides. Linear Cu_3Sn thickness change was found on both the anode and cathode sides after extended current stressing time, which is a result of the near constant-rate mass transport of controlling species, driven by the EM effect which was superimposed on the chemical potentials. Divergences of the mass transport rate across critical interfaces were the cause of two types of damage. At the Cu_6Sn_5/Sn interface of the cathode side, over-consumption of Cu dissolving into the solder caused the vacancy accumulation, thus initiating the crack; the propagation of the crack then caused the deterioration of the joint. At the Cu_3Sn/Cu_6Sn_5 interface of the anode side, compared with the thermal aging samples, the electric current caused Cu to flow back into Cu_3Sn, and hence the thickening of Cu_3Sn resulted in pores in the Cu_6Sn_5 layer near the interface. This study is expected to further elucidate fundamental behavior of microstructure evolution, and joint deteriorating mechanisms, for solder joint reliability under intensified current stressing conditions.

ACKNOWLEDGEMENTS

This work was supported by the National Natural Science Foundation of China (No. 51605498), National Basic Research Program of China (973 Program No. 2015CB057206), State Key Laboratory of High Performance Complex Manufacturing (ZZYJKT2016-08) and China Postdoctoral Science Foundation (2016M590752).

REFERENCES

1. B. Lee, J. Park, J. Song, K.-W. Kwon, and H.-J. Lee, *J. Electron. Mater.* 40, 324 (2010).
2. W. Zhang, *Jpn. J. Appl. Phys.* 54, 030203 (2015).
3. E.C.C. Yeh, W.J. Choi, K.N. Tu, P. Elenius, and H. Balkan, *Appl. Phys. Lett.* 80, 580 (2002).
4. K.N. Tu, *Microelectron. Reliab.* 51, 517 (2011).
5. B. Chao, S.-H. Chae, X. Zhang, K.-H. Lu, J. Im, and P.S. Ho, *Acta Mater.* 55, 2805 (2007).
6. Y.H. Lin, C.M. Tsai, Y.C. Hu, Y.L. Lin, and C.R. Kao, *J. Electron. Mater.* 34, 27 (2005).
7. H. Hsu, T.-Y. Lin, and F.-Y. Ouyang, *J. Electron. Mater.* 43, 236 (2013).
8. Y.L. Lin, C.W. Chang, C.M. Tsai, C.W. Lee, and C.R. Kao, *J. Electron. Mater.* 35, 1010 (2006).
9. J.H. Ke, T.L. Yang, Y.S. Lai, and C.R. Kao, *Acta Mater.* 59, 2462 (2011).
10. J.H. Ke, H.Y. Chuang, W.L. Shih, and C.R. Kao, *Acta Mater.* 60, 2082 (2012).
11. T.L. Yang, J.H. Ke, W.L. Shih, Y.S. Lai, and C.R. Kao, *J. Appl. Phys.* 114, 053501 (2013).
12. Y. Yao, L.M. Keer, and M.E. Fine, *J. Appl. Phys.* 105, 063710 (2009).
13. L.D. Chen, M.L. Huang, and S.M. Zhou, *J. Alloys Compd.* 504, 535 (2010).
14. Y.T. Huang, C.H. Chen, B.H. Lee, H.C. Chen, C.M. Wang, and A.T. Wu, *J. Electron. Mater.* 45, 6163 (2016).
15. C.-E. Ho, P.-T. Lee, C.-N. Chen, and C.-H. Yang, *J. Alloys Compd.* 676, 361 (2016).
16. F.-Y. Ouyang, H. Hsu, Y.-P. Su, and T.-C. Chang, *J. Appl. Phys.* 112, 023505 (2012).
17. H. Gan and K.N. Tu, *J. Appl. Phys.* 97, 063514 (2005).
18. M.-H. Jeong, G.-T. Lim, B.-J. Kim, K.-W. Lee, J.-D. Kim, Y.-C. Joo, and Y.-B. Park, *J. Electron. Mater.* 39, 2368 (2010).
19. Y. Jung and J. Yu, *J. Appl. Phys.* 115, 083708 (2014).
20. K. Meier, M. Roellig, S. Wiese, and C. Goette, in *International Conference on Thermal, Mechanical and Multi-*

Physics Simulation Experiments in Microelectronics and Micro-Systems. (Eurosime, 2007), pp. 1.
21. M.K. Rahman, A.M.M. Musa, B. Neher, K.A. Patwary, M.A. Rahman, and M.S. Islam, *J. Electron. Cool. Therm. Control* 06, 19 (2016).
22. L. Zhang, X.-Y. Fan, C.-W. He, and Y.-H. Guo, *J. Mater. Sci. Mater. Electron.* 24, 3249 (2013).
23. P.L. Tu, Y.C. Chan, K.C. Hung, and J.K.L. Lai, *Scripta Mater.* 44, 317 (2001).
24. Y. Yang, Y. Li, H. Lu, C. Yu, and J. Chen, *Microelectron. Reliab.* 53, 327 (2013).
25. Database for Solder Properties with Emphasis on New Lead-free Solders. (National Institute of Standards and Technology & Colorado School of Mines, 2002), https://www.metallurgy.nist.gov/solder/NIST_LeadfreeSolder_v4.pdf. Accessed 31 May 2017.
26. L. Mo, Z. Chen, F. Wu, and C. Liu, *Intermetallics* 66, 13 (2015).
27. Y. Yang, H. Lu, C. Yu, and Y. Li, *Microelectron. Reliab.* 51, 2314 (2011).
28. B. Chao, S.-H. Chae, X. Zhang, K.-H. Lu, M. Ding, J. Im, and P.S. Ho, *J. Appl. Phys.* 100, 084909 (2006).
29. J. Zhang and G.Q. Zhang, *Solid State Lighting Reliability Part 2: Components to Systems*, ed. W.K.V. Driel, X. Fan, and G.Q. Zhang (Cham: Springer, 2018), p. 337.
30. C. Chen and S.W. Liang, *J. Mater. Sci. Mater. Electron.* 18, 259 (2007).